Charge Transport in Photofunctional Nanoparticles Self-Assembled from Zinc 5,10,15,20-Tetrakis(perylenediimide)porphyrin Building Blocks

6 **AUTHORS**, INCLUDING:

Tamar van der boom

3 PUBLICATIONS   388 CITATIONS

SEE PROFILE

Ryan Hayes

Andrews University

18 PUBLICATIONS   1,536 CITATIONS

SEE PROFILE

Emily Weiss

Northwestern University

91 PUBLICATIONS   3,205 CITATIONS

SEE PROFILE

Charge Transport in Photofunctional Nanoparticles Self-Assembled from Zinc 5,10,15,20-Tetrakis(perylenediimide)porphyrin Building Blocks

Tamar van der Boom, Ryan T. Hayes, Yongyu Zhao, Patrick J. Bushard, Emily A. Weiss, and Michael R. Wasielewski*

Contribution from the Department of Chemistry and Center for Nanofabrication and Molecular Self-Assembly, Northwestern University, Evanston, Illinois 60208-3113

Received March 22, 2002

Abstract: Molecules designed to carry out photochemical energy conversion typically employ several sequential electron transfers, as do photosynthetic proteins. Yet, these molecules typically do not achieve the extensive charge transport characteristic of semiconductor devices. We have prepared a large molecule in which four perylene-3,4:9,10-tetracarboxydiimide (PDI) molecules that both collect photons and accept electrons are attached to a central zinc 5,10,15,20-tetraphenylporphyrin (ZnTPP) electron donor. This molecule self-assembles into ordered nanoparticles both in solution and in the solid-state, driven by van der Waals stacking of the PDI molecules. Photoexcitation of the nanoparticles results in quantitative charge separation in 3.2 ps to form ZnTPP$^+$PDI$^-$ radical ion pairs, in which the radical anion rapidly migrates to PDI molecules that are, on average, 21 Å away, as evidenced by magnetic field effects on the yield of the PDI triplet state that results from radical ion pair recombination. These nanoparticles exhibit charge transport properties that combine important features from both photosynthetic and semiconductor photoconversion systems.

Introduction

The successful development of molecular devices for applications in photochemical energy conversion and storage as well as molecular electronics requires fundamental research into the distinctly different physical phenomena that occur on nanometer length scales. Artificial photosynthetic systems[1,2] as well as single molecules specifically designed for applications as switches, wires, and rectifiers have been studied.[3–15] Over the past few years, we have developed several approaches to controlling charge transport in organic nanostructures that take advantage of the speed and efficiency of ultrafast photoinduced electron-transfer reactions.[16–18] A critical step toward photofunctional devices is the ability to create increasingly larger arrays of interactive molecules. Covalent synthesis of large molecular arrays is highly inefficient and costly, thus making self-assembly the method of choice to achieve ordered architectures from functional building blocks. Self-assembly can be based on a variety of weak interactions, such as hydrogen bonding[19–23] and π–π van der Waals interactions[24,25] as well as covalent bonds.[26–28]

* Address correspondence to this author. E-mail: wasielew@chem.northwestern.edu.
(1) Wasielewski, M. R. *Chem. Rev.* **1992**, *92*, 435−461.
(2) Gust, D.; Moore, T. A.; Moore, A. L. *Acc. Chem. Res.* **2001**, *34*, 40−48.
(3) Wagner, R. W.; Lindsey, J. S.; Seth, J.; Palaniappan, V.; Bocian, D. F. *J. Am. Chem. Soc.* **1996**, *118*, 3996−3997.
(4) de Silva, A. P.; Gunaratne, H. Q. N.; Gunnlaugsson, T.; Huxley, A. J. M.; McCoy, C. P.; Radmacher, J. T.; Rice, T. E. *Chem. Rev.* **1997**, *97*, 1515−1566.
(5) Willner, I.; Willner, B. *J. Mater. Chem.* **1998**, *8*, 2543−2556.
(6) Tour, J. M.; Kozaki, M.; Seminario, J. M. *J. Am. Chem. Soc.* **1998**, *120*, 8486−8493.
(7) Collier, C. P.; Mattersei, G.; Wong, E. W.; Luo, Y.; Beverly, K.; Sampaio, J.; Raymo, F. M.; Stoddart, J. F.; Heath, J. R. *Science* **2000**, *289*, 1172−1175.
(8) Davis, W. B.; Svec, W. A.; Ratner, M. A.; Wasielewski, M. R. *Nature* **1998**, *396*, 60−63.
(9) Waldeck, D. H.; Beratan, D. N. *Science* **1993**, *261*, 576−577.
(10) Metzger, R. M. *Acc. Chem. Res.* **1999**, *32*, 950−957.
(11) Chen, J.; Reed, M. A.; Rawlett, A. M.; Tour, J. M. *Science* **1999**, *286*, 1550−1552.
(12) Prathapan, S.; Yang, S. I.; Seth, J.; Miller, M. A.; Bocian, D. F.; Holten, D.; Lindsey, J. S. *J. Phys. Chem. B* **2001**, *105*, 8237−8248.
(13) Yang, S. I.; Prathapan, S.; Miller, M. A.; Seth, J.; Bocian, D. F.; Lindsey, J. S.; Holten, D. *J. Phys. Chem. B* **2001**, *105*, 8249−8258.
(14) Ik Yang, S.; Lammi, R. K.; Prathapan, S.; Miller, M. A.; Seth, J.; Diers, J. R.; Bocian, D. F.; Lindsey, J. S.; Holten, D. *J. Mater. Chem.* **2001**, *11*, 2420−2430.
(15) del Rosario Benites, M.; Johnson, T. E.; Weghorn, S.; Yu, L.; Rao, P. D.; Diers, J. R.; Yang, S. I.; Kirmaier, C.; Bocian, D. F.; Holten, D.; Lindsey, J. S. *J. Mater. Chem.* **2002**, *12*, 65−80.
(16) Gosztola, D.; Niemczyk, M. P.; Wasielewski, M. R. *J. Am. Chem. Soc.* **1998**, *120*, 5118−5119.
(17) Hayes, R. T.; Wasielewski, M. R.; Gosztola, D. *J. Am. Chem. Soc.* **2000**, *122*, 5563−5567.
(18) Lukas, A. S.; Bushard, P. J.; Wasielewski, M. R. *J. Am. Chem. Soc.* **2001**, *123*, 2440−2441.
(19) Kotera, M.; Lehn, J.-M.; Vigneron, J.-P. *Tetrahedron* **1995**, *51*, 1953−1972.
(20) Sessler, J. L.; Wang, B.; Harriman, A. *J. Am. Chem. Soc.* **1995**, *117*, 704−714.
(21) Springs, S. L.; Andrievsky, A.; Kral, V.; Sessler, J. L. *J. Porphyrins Phthalocyanines* **1998**, *2*, 315−325.
(22) Arimura, T.; Ide, S.; Sugihara, H.; Murata, S.; Sessler, J. L. *New J. Chem.* **1999**, *23*, 977−979.
(23) Berg, A.; Shuali, Z.; Asano-Someda, M.; Levanon, H.; Fuhs, M.; Moebius, K.; Wang, R.; Brown, C.; Sessler, J. L. *J. Am. Chem. Soc.* **1999**, *121*, 7433−7434.
(24) Shimomura, M.; Olaf, K.; Ijiro, K. *Synth. Met.* **1996**, *81*, 251−257.
(25) Zangmeister, R. A. P.; Smolenyak, P. E.; Drager, A. S.; O'Brien, D. F.; Armstrong, N. R. *Langmuir* **2001**, *17*, 7071−7078.
(26) Mirkin, C. A.; Ratner, M. A. *Molecular Electronics*; Annual Reviews Inc.: Palo Alto, CA, 1992; Vol. 43.

Chart 1

ZnTPP-PDI₄

PDI₂

ZnTPP-PDI

ZnTPP-PDI₂

R = 3,5-di-t-butylphenoxy   R' = 2-ethylhexyl
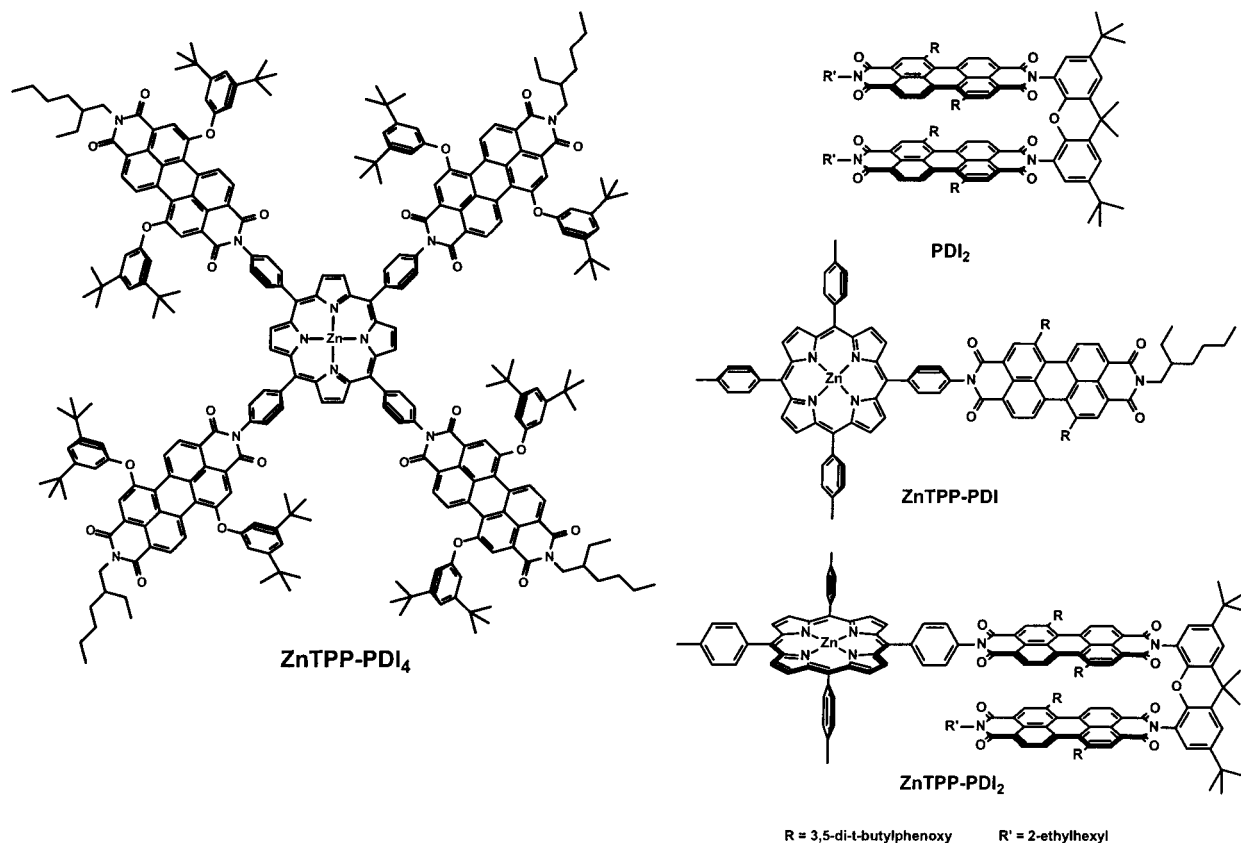
Photosynthesis is an important model for efficient photochemical energy conversion. Antenna proteins in photosynthetic organisms contain many chlorophylls that increase the cross section for absorption of light.[29] Light absorption by antenna chlorophylls creates singlet excitons that migrate very rapidly among these chlorophylls. Some of the excitons are eventually trapped by the primary electron donor chlorophyll within a nearby reaction center protein, leading to charge separation in a few picoseconds. The protein environment in the vicinity of each chlorophyll cofactor as well as its proximity to electron donors or acceptors largely determines whether it acts as an antenna chromophore or a redox agent. In contrast to stepwise charge separation in photosynthetic proteins, photoconversion using dye-sensitized semiconductors depends on ultrafast electron injection from the photoexcited dye into the conduction band of the semiconductor, followed by rapid charge transport throughout the semiconductor structure.[30−36]

We now report on a zinc 5,10,15,20-tetrakis(perylenediimide)-porphyrin, ZnTPP−PDI₄ (Chart 1), that self-assembles into ordered photofunctional organic nanoparticles using van der Waals interactions between the individual molecules and not only exhibits the characteristics of an antenna-reaction center complex described above but demonstrates more extensive charge transport within the nanoparticles as well.

Results and Discussion

Synthesis. Four perylene-3,4:9,10-tetracarboxydiimide (PDI) molecules, which act as both antenna pigments and electron acceptors, are covalently bound to a central zinc *meso*-tetraphenylporphyrin (ZnTPP) electron donor to give ZnTPP−PDI₄. The known 1,7-dibromoperylene-3,4:9,10-tetracarboxy-dianhydride[37] is reacted with 3,5-di-*tert*-butylphenol in the presence of Cs₂CO₃ in refluxing DMF to yield the corresponding 1,7-diphenoxylated perylene-3,4:9,10-tetracarboxydianhydride (PDA) chromophore. The phenoxy groups serve to greatly increase the solubility of the PDA molecule and derivatives made from it.[38] Reaction of PDA with an equivalent of 2-ethylhexylamine yields the corresponding imide-anhydride (PIA). An 8-fold excess of PIA is reacted with 5,10,15,20-tetrakis(*p*-aminophenyl)porphyrin[39] over a period of 4 days in refluxing pyridine containing 30% (w/v) imidazole (Im) to give a 44% yield of the free base TPP−PDI₄. We have found that

(27) Wiederrecht, G. P.; Yoon, B. A.; Svec, W. A.; Wasielewski, M. R. *J. Am. Chem. Soc.* **1997**, *119*, 3358−3364.
(28) Ramos, A. M.; Rispens, M. T.; van Duren, J. K. J.; Hummelen, J. C.; Janssen, R. A. J. *J. Am. Chem. Soc.* **2001**, *123*, 6714−6715.
(29) Diner, B. A.; Babcock, G. T. *Adv. Photosynth.* **1996**, *4*, 213−247.
(30) Desilvestro, J.; Grätzel, M.; Kavan, L.; Moser, J.; Augustynski, J. *J. Am. Chem. Soc.* **1985**, *107*, 2988−2990.
(31) Nazeeruddin, M. K.; Kay, A.; Rodicio, I.; Humphrey-Baker, R.; Müller, E.; Liska, P.; Vlachopoulos, N.; Grätzel, M. *J. Am. Chem. Soc.* **1993**, *115*, 6382−6390.
(32) Martini, I.; Hodak, J. H.; Hartland, G. V. *J. Phys. Chem. B* **1999**, *103*, 9104−9111.
(33) Hasselmann, G. M.; Meyer, G. J. *J. Phys. Chem. B* **1999**, *103*, 7671−7675.
(34) Haque, S. A.; Tachibana, Y.; Willis, R. L.; Moser, J. E.; Grätzel, M.; Klug, D. R.; Durrant, J. R. *J. Phys. Chem.* **2000**, *104*, 53−547.
(35) Nazeeruddin, M. K.; P. Péchy, T. R.; Zakeeruddin, S. M.; Humphrey-Baker, R.; Comte, P.; Liska, P.; Cevey, L.; Costa, E.; Shklover, V.; Spiccia, L.; Deacon, G. B.; Bignozzi, C. A.; Grätzel, M. *J. Am. Chem. Soc.* **2001**, *123*, 1613−1624.

(36) Asbury, J. B.; Hao, E.; Wang, Y.; Ghosh, H. N.; Lian, T. *J. Phys. Chem. B* **2001**, *105*, 4545−4557.
(37) Bohm, A.; Arms, H.; Henning, G.; Blaschka, P. (BASF). German Patent No. DE 19547209A1, 1997.
(38) Quante, H.; Geerts, Y.; Mullen, K. *Chem. Mater.* **1997**, *9*, 495−500.
(39) Bettleheim, A.; White, B. A.; Raybuck, S. A.; Murray, R. W. *Inorg. Chem.* **1987**, *26*, 1009−1017.

25−40% (w/v) imidazole in chloroform or pyridine produces reasonable yields of imide formation with minimal decomposition of the starting materials. Zinc insertion into TPP−PDI$_4$ occurs readily using zinc acetate in chloroform/methanol to yield ZnTPP−PDI$_4$.

Several reference molecules were also prepared to aid in understanding the properties of ZnTPP−PDI$_4$. A ZnTPP bound to a single PDI molecule, ZnTPP−PDI, was prepared in a manner similar to that of ZnTPP−PDI$_4$ by reacting a slight excess of PIA with 5-(*p*-aminophenyl)-10,15,20-tris(*p*-tolyl)-porphyrin.[40] In addition, two molecules in which a pair of PDI molecules are constrained to a cofacial orientation were also prepared. A 3-fold molar excess of PIA was reacted with 2,7-di-*tert*-butyl-9,9-dimethyl-4,5-xanthenediamine[41] to yield the face-to-face dimer PDI$_2$. Reacting a 2.5 molar excess of the xanthenediamine with PIA gave the PDI-Xan-NH$_2$. Reaction of 5-(*p*-aminophenyl)-10,15,20-tris(*p*-tolyl)porphyrin with a 3-fold molar excess of PDA in refluxing CHCl$_3$/Im yielded the porphyrin−PIA molecule, TPP−PIA, with a terminal anhydride. Reaction of a 3-fold molar excess of TPP−PIA with PDI-Xan-NH$_2$ in refluxing CHCl$_3$/Im gave TPP−PDI$_2$, which was metalated with ZnOAc$_2$ in CHCl$_3$/MeOH to give ZnTPP−PDI$_2$. Details regarding the preparation and characterization of these molecules are given in the Supporting Information.

Self-Assembled Nanoparticles. The mass spectrum of ZnTPP−PDI$_4$ obtained using MALDI/TOF techniques is shown in Figure 1. This spectrum shows peaks at multiples of the *m/z* = 4310 parent ion up to about 80 kD, which are assemblies of about 20 molecules. This spectrum provides direct evidence for the strong tendency of ZnTPP−PDI$_4$ to self-assemble, even in the gas phase. Dynamic light-scattering measurements on a 10^{-4} M solution of ZnTPP−PDI$_4$ in toluene using 632.8 nm light shows that this molecule also forms large soluble nanoparticles with a 150 ± 30 nm diameter, assuming a spherical particle model. The nanoparticle size decreases with decreasing concentration, reaching 40 nm at 10^{-5} M, which is the limit of our light-scattering measurements. The strong tendency of ZnTPP−PDI$_4$ to self-assemble in solution to form (ZnTPP−PDI$_4$)$_n$ nanoparticles is also evidenced by its proton NMR spectrum, which displays broadened lines in chloroform, dimethyl sulfoxide, and pyridine at temperatures up to 100 °C and at concentrations down to 10^{-5} M. The proton NMR spectrum of the (ZnTPP−PDI$_4$)$_n$ nanoparticles in CDCl$_3$ at 50 °C is shown in the Supporting Information. In contrast, the NMR and mass spectra of ZnTPP, ZnTPP−PDI, and ZnTPP−PDI$_2$ show that these molecules do not self-associate in solution.

The optical absorption spectrum of ZnTPP−PDI in toluene (Figure 2) clearly shows the ZnTPP B band at 424 nm and the lowest energy Q-band at 592 nm, along with an intense band at 550 nm due to the PDI molecule with its lower intensity vibronic band at 509 nm. Comparing the PDI bands within ZnTPP−PDI to those of the (ZnTPP−PDI$_4$)$_n$ nanoparticles, the ZnTPP B bands are very similar, while the (ZnTPP−PDI$_4$)$_n$ nanoparticles exhibit a new intense 515 nm PDI band. If the transition dipoles of two identical chromophores are positioned in a parallel, stacked geometry, the molecular exciton model
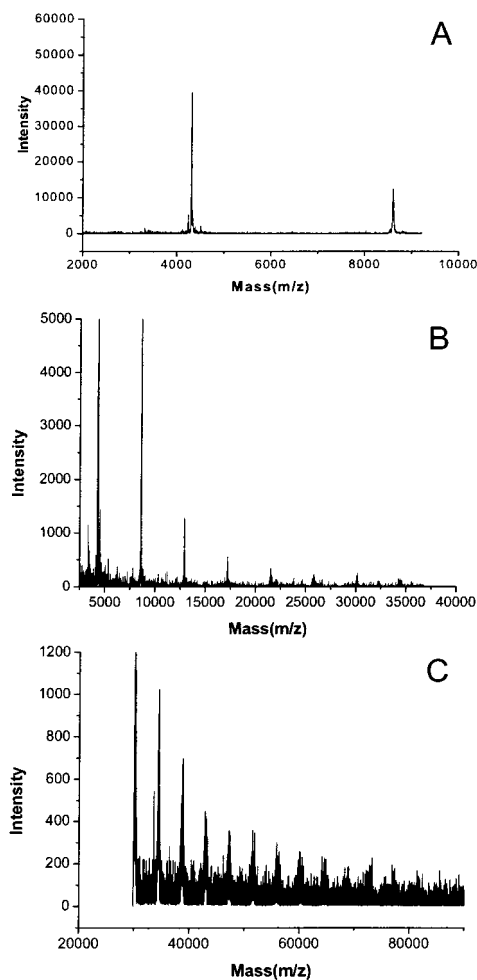

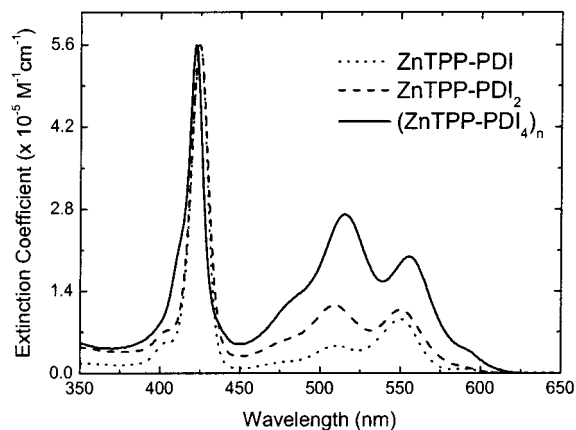**Figure 1.** MALDI/TOF mass spectra of (ZnTPP−PDI$_4$)$_n$ at three different mass ranges.

Figure 2. Optical absorption spectra of ZnTPP−PDI, ZnTPP−PDI$_2$, and (ZnTPP−PDI$_4$)$_n$ in toluene.

predicts that coupling of the two transition dipoles will cause the lowest energy electronic transition of the dimer to split into two bands, with the higher energy band having all of the oscillator strength.[42] The presence of the intense 515 nm band in (ZnTPP−PDI$_4$)$_n$ suggests that the PDI molecules in this nanoparticle adopt a parallel, stacked geometry, while the lack of a significant bandshift and/or splitting for the ZnTPP

(40) Gust, D.; Moore, T. A.; Moore, A. L.; Gao, F.; Luttrull, D.; DeGraziano, J. M.; Ma, X. C.; Makings, L. R.; Lee, S. J.; et al. *J. Am. Chem. Soc.* **1991**, *113*, 3638−3649.

(41) Hamann, B. C.; Branda, N. R.; Rebek, J. *Tetrahedron Lett.* **1993**, *34*, 6837−6840.

(42) Kasha, M.; Rawls, H. R.; El-Bayoumi, M. A. *Pure Appl. Chem.* **1965**, *11*, 371−392.
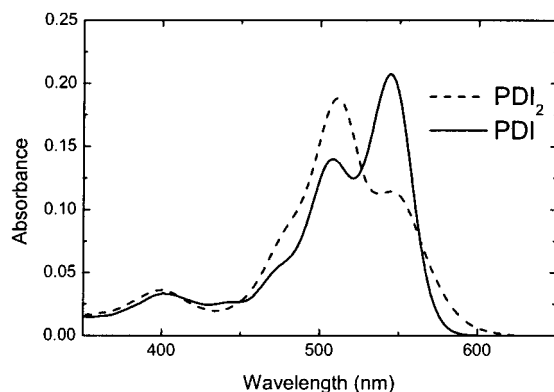
Figure 3. Optical absorption spectra of PDI and PDI_2 in toluene.

molecules suggests that they have a relative distance and/or geometry in which exciton coupling is weak.

To test this hypothesis, we prepared PDI_2 and $ZnTPP-PDI_2$, in which two PDI chromophores are constrained by a diaminoxanthene spacer molecule[41] to a parallel, stacked geometry, which places the transition dipoles for the 550 nm transitions in the PDI chromophores parallel to one another. Apart from differences in extinction coefficients due to the ZnTPP/PDI ratio, the optical spectra of $ZnTPP-PDI_2$ and the $(ZnTPP-PDI_4)_n$ nanoparticles in toluene shown in Figure 2 exhibit PDI bands very similar to each other and to those of PDI_2 in Figure 3. Face-to-face stacking of an infinite number of chromophores will increase the exciton splitting by no more than a factor of 2 beyond that of the dimer, but this increase will be masked somewhat by the broad bandwidth of the transitions.[42] A comparison of the optical absorption spectra of PDI and PDI_2 in Figure 3 shows that PDI_2 exhibits a new, intense band at 511 nm, which agrees well with the predictions of the molecular exciton model.[42] However, the optical transition from the ground state of PDI_2 to the lower exciton state, which is symmetry forbidden in the molecular exciton model for the dimer geometry enforced by the xanthene spacer in PDI_2, still has significant oscillator strength, as evidenced by the intensity of the band at 550 nm. Extension of the simple molecular exciton model to include vibronic coupling in the exciton states of the dimer relieves the symmetry restrictions inherent to the simple model.[43,44] Thus, the 511 nm band is the transition from the ground state to the $v = 0$ vibronic level of the upper exciton state, while the 550 nm band is the corresponding transition to the $v = 1$ vibronic level of the lower exciton state. The greater oscillator strength of the 511 nm transition in PDI_2 is consistent with the geometry of the dimer enforced by the xanthene spacer. The presence of the low-energy transition is also evident in the spectra of $ZnTPP-PDI_2$ and the $(ZnTPP-PDI_4)_n$ nanoparticles.

Remarkably, the optical absorption spectrum of $(ZnTPP-PDI_4)_n$ in pyridine is very similar to that observed in toluene (Figure 4A). The $(ZnTPP-PDI_4)_n$ nanoparticles are stable toward coordination of ligands to the ZnTPP core. Pyridine coordinates to the Zn within the ZnTPP core *without significantly disrupting the nanoparticles*. This suggests that the self-assembly process is driven primarily by an interaction between the PDI molecules. Titration of pyridine into a toluene solution
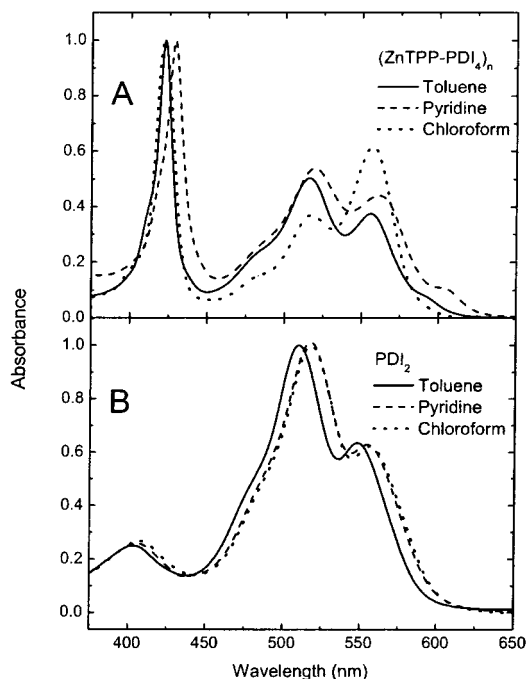
(43) Fulton, R. L.; Gouterman, M. *J. Chem. Phys.* **1964**, *41*, 2280−2286.
(44) Oddos-Marcel, L.; Madeore, F.; Bock, A.; Neher, D.; Ferencz, A.; Rengel, H.; Wegner, G.; Kryschi, C.; Trommsdorff, H. P. *J. Phys. Chem.* **1996**, *100*, 11850−11856.

Figure 4. Comparison of optical absorption spectra in toluene, pyridine, and chloroform: (A) $(ZnTPP-PDI_4)_n$ and (B) PDI_2.

of 10^{-5} M $(ZnTPP-PDI_4)_n$ nanoparticles results in a red shift of the ZnTPP Soret band from 422 (toluene) to 429 nm (toluene: pyridine = 5:3 v/v). In addition, the lowest energy Q_y band of ZnTPP moves to about 600 nm and increases in intensity, as is typical for ZnTPP with a pyridine ligand.[45] These observations strongly suggest that pyridine can easily access the ZnTPP molecules within the $(ZnTPP-PDI_4)_n$ nanoparticles.

In contrast to the behavior of pyridine, addition of $CHCl_3$ (free of ethanol) to a toluene solution of the $(ZnTPP-PDI_4)_n$ nanoparticles disassembles the particles to a large extent. The optical spectra obtained in toluene and $CHCl_3$ are compared directly in Figure 4A. Except for differences in the relative extinction coefficients due to the ZnTPP/PDI ratio, the spectrum in $CHCl_3$ resembles that of ZnTPP−PDI, which does not form larger structures. However, the proton NMR spectrum of $ZnTPP-PDI_4$ in $CDCl_3$ displays broadened lines, especially the PDI resonances, which are shifted upfield from their positions in ZnTPP−PDI, indicating that some degree of PDI stacking leading to small oligomers of $ZnTPP-PDI_4$ most likely occurs in chloroform. If the chloroform is removed in vacuo, and the $ZnTPP-PDI_4$ is redissolved in toluene, the optical absorption spectrum and light-scattering measurements show that the self-assembled nanoparticles are restored, indicating that the self-assembly process is completely reversible. By comparison, if PDI_2 is dissolved in chloroform, its optical absorption spectrum is only slightly red shifted and is very similar to that of PDI_2 in toluene (Figure 4B). This is consistent with the parallel transition dipole orientation enforced by the xanthene spacer, which does not depend on the solvent.

The optical spectra strongly support the proposed structure of the $(ZnTPP-PDI_4)_n$ nanoparticles depicted schematically in Figure 5A. The PDI molecules most likely stack directly on top of one another in register, presumably at a van der Waals contact distance of about 3.5 Å, while the ZnTPP molecules

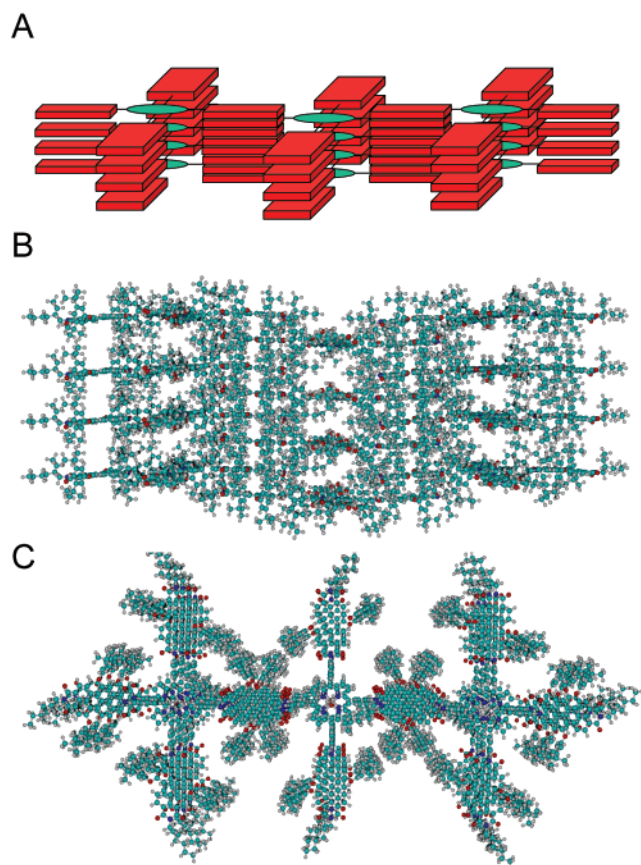(45) Nappa, M.; Valentine, J. S. *J. Am. Chem. Soc.* **1978**, *100*, 5075−5080.

Figure 5. (A) Cartoon of the structure of self-assembled (ZnTPP−PDI$_4$)$_{12}$ nanoparticles. (B, C) Top and side views, respectively, of the energy-minimized structure of (ZnTPP−PDI$_4$)$_{12}$ nanoparticles determined using MM+ force field calculations.

occupy sites in every other layer, with an interlayer Zn−Zn distance of about 7 Å. At this distance, the exciton interaction between two metalloporphyrins is less than 150 cm^{-1}, in agreement with the experimental observation.[46] Although other structures cannot be rigorously excluded, the proposed structure allows enough space between the ZnTPP molecules for the observed ligation of pyridine to ZnTPP without disrupting the PDI stacking. The proposed structure of a (ZnTPP−PDI$_4$)$_n$ nanoparticle for which $n = 12$ was obtained using an MM+ force field calculation and is shown in Figure 5B,C.[47] Thus far, all attempts to obtain single crystals of the (ZnTPP−PDI$_4$)$_n$ nanoparticles sufficiently large for X-ray diffraction studies have failed.

Spin-coating a 10^{-4} M solution of (ZnTPP−PDI$_4$)$_n$ nanoparticles in toluene onto a quartz slide that has been pretreated with CH$_3$SiCl$_3$ to render the surface hydrophobic results in the deposition of cone-shaped structures that average 30−50 nm in height and 100−150 nm in diameter at the base, as determined by atomic force microscopy (AFM) (Figure 6). In addition, spin-coating the ZnTPP−PDI and ZnTPP−PDI$_2$ reference molecules onto a methylsilylated quartz surface does not result in the formation of cone-shaped structures, as indicated by AFM. Figure 7 shows the spectrum of the 150 nm (ZnTPP−PDI$_4$)$_n$ nanoparticles spin-coated onto the methylsilylated quartz surface.

(46) Senge, M. O.; Gerzevske, K. R.; Vicente, M. G. H.; Forsyth, T. P.; Smith, K. M. *Angew. Chem., Int. Ed. Engl.* **1993**, *32*, 750−753.
(47) MM+, AM1, and ZINDO/S calculations were performed using HyperChem-(TM), Hypercube, Inc., 1115 NW 1114th St., Gainesville, FL 32601.
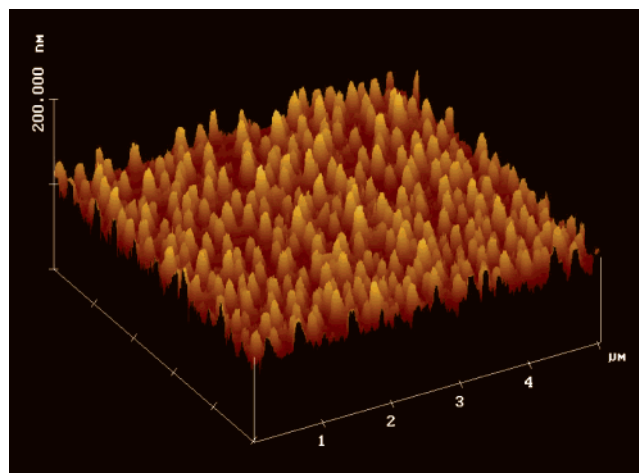
Figure 6. Atomic force micrograph of a CH$_3$SiCl-treated quartz plate over which (ZnTPP−PDI$_4$)$_n$ nanoparticles were deposited by spin-coating.
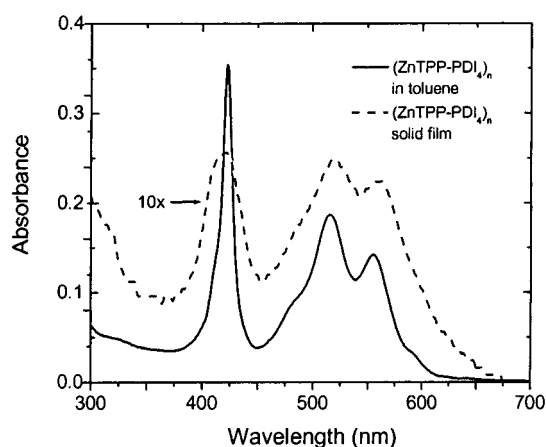

Figure 7. Optical absorption spectra of (ZnTPP−PDI$_4$)$_n$ nanoparticles in toluene and in a solid film.

All of the spectral features characteristic of (ZnTPP−PDI$_4$)$_n$ nanoparticles in solution, including the dominant 515 nm band, are present in the spectra of the cone-shaped solid particles. This suggests that the parallel, stacked structural motif for the PDI molecules within (ZnTPP−PDI$_4$)$_n$ is present both in solution and in the solid. Given the proposed interleaved structure in Figure 5, the ZnTPP molecules form an array in which the lateral Zn−Zn spacing is 30 Å and the Zn−Zn distance along the stacking direction is 7 Å. Thus, the cone-shaped structures in Figure 6 that are 50 nm tall and have a 150 nm diameter base should contain approximately 6 × 10^4 ZnTPP−PDI$_4$ molecules.

Photoinduced Charge Transport. The PDI molecule acts as a good antenna chromophore, with a lowest excited singlet state that has an energy of $E_S = 2.25$ eV, a fluorescence quantum yield of unity, and a lifetime of $\tau = 4.5$ ns. As a consequence of PDI stacking, the lower exciton state energy of the PDI molecules in ZnTPP−PDI$_2$ and the (ZnTPP−PDI$_4$)$_n$ nanoparticles is 2.15 eV. Thus, singlet−singlet energy transfer to ZnTPP, for which $E_S = 2.06$ eV, should be facile in ZnTPP−PDI, ZnTPP−PDI$_2$, and (ZnTPP−PDI$_4$)$_n$. In addition, PDI is an excellent electron acceptor, with a reversible redox potential for one-electron reduction of −0.53V vs saturated calomel electrode. The free energy of reaction for photoinduced electron transfer from ^{1*}ZnTPP to PDI is $\Delta G = E_{OX} - E_{RED} - E_S - e_o^2/r\epsilon_S + S$, where E_{OX} and E_{RED} are the one-electron oxidation
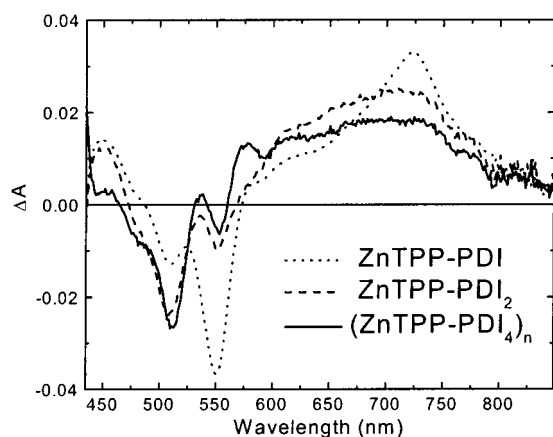
Figure 8. Transient absorption spectra of 10^{-4} M ZnTPP–PDI, ZnTPP–PDI$_2$, and (ZnTPP–PDI$_4$)$_n$ in toluene at 100 ps following a 420 nm, 130 fs laser flash. The spectra are normalized for both excitation energy and sample concentration.

Figure 9. Spectroelectrochemical difference spectra, ground state subtracted from the radical anion state, for PDI and PDI$_2$ in DMF containing 0.1 M tetra-n-butylammonium perchlorate.

and reduction potentials for ZnTPP (0.82 V vs SCE) and PDI, respectively, e_o is the electronic charge, r is the distance between the ions (14.4 Å), ϵ_S is the static dielectric constant of the medium ($\epsilon_S = 2.4$ for toluene), and S is the difference between the energies of the ion pair product in the polar solvent in which E_{OX} and E_{RED} are measured and in other less polar solvents in which the electron-transfer rate constants are measured.[48] The value of ΔG for the reaction ^{1*}ZnTPP–PDI $\rightarrow$ ZnTPP$^+$–PDI$^-$ in butyronitrile, a polar solvent wherein $e_o^2/r\epsilon_S \cong S \cong 0$, is -0.71 eV, while ΔG is about -0.3 eV in toluene, a lower polarity solvent.[48]

Photoinduced electron transfer within the 150 nm (ZnTPP–PDI$_4$)$_n$ nanoparticles as well as within the ZnTPP–PDI and ZnTPP–PDI$_2$ reference molecules in toluene was examined using femtosecond transient absorption spectroscopy. The absorbance of ZnTPP is at least 30 times greater than that of the PDI species within each of these molecules at 420 nm, so that selective excitation of ZnTPP within each molecule was carried out with 420 nm, 130 fs laser pulses. Excitation of ZnTPP–PDI results in formation of ZnTPP$^+$–PDI$^-$, with $\tau = 15$ ps, as monitored by formation of the characteristic PDI$^-$ absorption band at 720 nm (Figure 8).[49] The ZnTPP$^+$–PDI$^-$ radical ion pair recombines, with $\tau = 5.3$ ns. Given that the lowest excited singlet state of ZnTPP has a 2.4 ns lifetime, the 15 ps time constant for charge separation within ZnTPP–PDI implies that this reaction occurs with >99% yield. Excitation of ZnTPP–PDI$_2$ with 420 nm laser pulses forms ZnTPP$^+$–PDI$_2^-$, with $\tau = 9.3$ ps, which also recombines, with $\tau = 5.3$ ns. However, the transient absorption spectrum of ZnTPP$^+$–PDI$_2^-$ (Figure 8) shows that the spectrum of PDI$_2^-$ is broadened and reduced in intensity relative to that of PDI$^-$. The nature of this broadening will be discussed below. Excitation of the 150 nm (ZnTPP–PDI$_4$)$_n$ nanoparticles with 420 nm laser pulses results in formation of ZnTPP$^+$–PDI$_4^-$(ZnTPP–PDI$_4$)$_{n-1}$, with $\tau = 3.2$ ps, followed by radical ion pair recombination with $\tau = 7.2$ ns. Thus, the expected statistical shortening of the overall charge separation time constant occurs in these molecules as more PDI molecules are attached to the ZnTPP core. When the
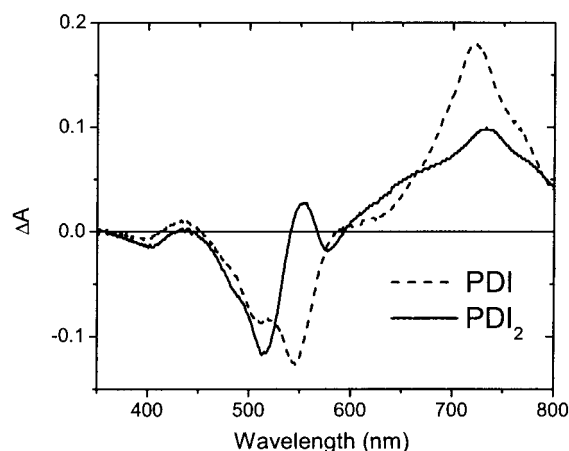
(48) Lukas, A. S.; Miller, S. E.; Wasielewski, M. R. *J. Phys. Chem. B* **2000**, *104*, 931–940.
(49) Gosztola, D.; Niemczyk, M. P.; Svec, W. A.; Lukas, A. S.; Wasielewski, M. R. *J. Phys. Chem. A* **2000**, *104*, 6545–6551.

PDI molecules attached to ZnTPP are selectively excited with 515 nm, 130 fs laser pulses in ZnTPP, ZnTPP–PDI$_2$, and (ZnTPP–PDI$_4$)$_n$, the time constants for charge separation are indistinguishable from those obtained using 420 nm excitation. Thus, in each case energy transfer from ^{1*}PDI to ZnTPP occurs much faster than the time constant for charge separation.

The transient absorption spectra of the reduced PDI species in ZnTPP$^+$–PDI$_2^-$ and ZnTPP$^+$–PDI$_4^-$(ZnTPP–PDI$_4$)$_{n-1}$ are substantially broadened and reduced in intensity from the spectrum of ZnTPP$^+$–PDI$^-$ in the region from 650 to 750 nm. This may be due to delocalization of the negative charge from PDI$^-$ onto the other PDI molecules that are in van der Waals contact with it. To test this hypothesis, we performed spectro-electrochemical measurements on both PDI and PDI$_2$. The differences between the optical spectra of the corresponding radical anions and their ground-state spectra are shown in Figure 9. It is clear that the near-infrared optical spectra of the model radical anions are very similar to those of the photogenerated species shown in Figure 8.

To further examine the nature of the spectral broadening within PDI$_2^-$, we performed semiempirical, unrestricted Hartree–Fock calculations on the radical anions of both PDI and PDI$_2$ using the AM1 method to determine their energy-minimized ground-state structures.[47] In both molecules, the phenoxy groups were replaced by methoxy groups, and the octyl tails were replaced with hydrogen. The electronic spectra of the radical anions were calculated by applying ZINDO/S to the energy-minimized, AM1 ground-state structures of the radical anions.[47] We have shown previously that this protocol results in reasonably accurate estimates of the electronic transitions within the radical anions of PDI derivatives without the phenoxy groups at the 1 and 7 positions.[49] The calculated wavelength (and oscillator strength) of the transition that corresponds to that observed at 720 nm for PDI$^-$ is 674 nm (0.95), while the calculation for PDI$_2^-$ predicts two transitions at 692 (0.24) and 610 nm (0.53). The results of these calculations agree reasonably well with the observed absorption spectra of ZnTPP$^+$–PDI$_2^-$ and PDI$_2^-$ between 650 and 700 nm. The somewhat broader spectral features observed for ZnTPP$^+$–PDI$_4^-$(ZnTPP–PDI$_4$)$_{n-1}$ most likely arise from delocalization of the electron over two or more PDI molecules as well.
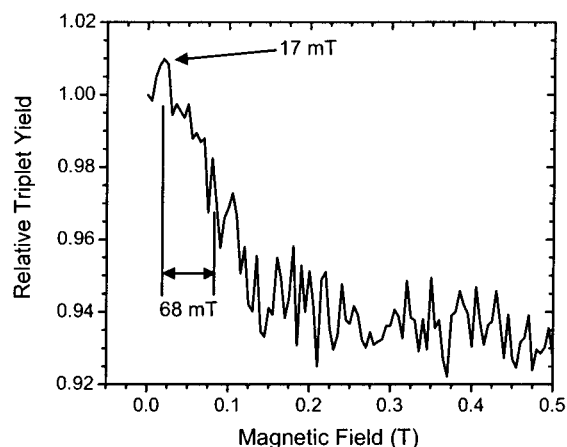
Figure 10. Magnetic field effect on the relative ^{3}*PDI yield within 10^{-4} M (ZnTPP−PDI$_4$)$_n$ nanoparticles in toluene. The triplet yield was determined by monitoring the transient absorption change at 480 nm at 100 ns following the laser flash. The relative triplet yield does not depend on the time during the lifetime of ^{3}*PDI that the yield is measured.

Charge recombination within ZnTPP$^+$−PDI$^−$, ZnTPP$^+$−PDI$_2{}^−$, and (ZnTPP$^+$−PDI$_4{}^−$)(ZnTPP−PDI$_4$)$_{n-1}$ produces not only the ground state but the neutral lowest excited triplet state, ^{3}*PDI, as well. Since the energy of ^{3}*PDI is 1.2 eV,[50] while that of ^{3}*ZnTPP is 1.7 eV,[51] the triplet state resulting from charge recombination resides on PDI, which was confirmed by nanosecond transient absorption spectroscopy.[50] If the photogenerated charge separation and the subsequent thermal recombination reactions are carried out in an applied magnetic field up to 1.2 T, the yield of ^{3}*PDI does not change for ZnTPP−PDI and ZnTPP−PDI$_2$, whereas the yield of ^{3}*PDI within the (ZnTPP−PDI$_4$)$_n$ nanoparticles increases to a maximum at 17 mT and then decreases by about 8% overall (Figure 10). The half-width at half-height of the magnetic field effect on the relative triplet yield is $B_{1/2} = 68$ mT.

The formation of ^{3}*PDI is a consequence of radical ion pair intersystem crossing within the initially formed singlet radical ion pair ^{1}(ZnTPP$^+$−PDI$_4{}^−$)(ZnTPP−PDI$_4$)$_{n-1}$.[52−54] The energies of the singlet and triplet radical ion pairs,^{1}(ZnTPP$^+$−PDI$_4{}^−$)-(ZnTPP−PDI$_4$)$_{n-1}$ and ^{3}(ZnTPP$^+$−PDI$_4{}^−$)(ZnTPP−PDI$_4$)$_{n-1}$, respectively, differ by the spin−spin exchange interaction, $2J$ (Figure 11). At zero magnetic field, if $2J \leq \sum a_i$, where a_i are the electron−nuclear hyperfine interactions within ZnTPP$^+$ and PDI$^−$, all three triplet sublevels of ^{3}(ZnTPP$^+$−PDI$_4{}^−$)(ZnTPP−PDI$_4$)$_{n-1}$ mix with the singlet ^{1}(ZnTPP$^+$−PDI$_4{}^−$)(ZnTPP−PDI$_4$)$_{n-1}$. On the other hand, if $2J \gg \sum a_i$ at zero magnetic field, no mixing occurs. Upon application of an external magnetic field, the Zeeman interaction splits the triplet sublevels of ^{3}-(ZnTPP$^+$−PDI$_4{}^−$)(ZnTPP−PDI$_4$)$_{n-1}$, which raises and lowers the energies of two of the three triplet sublevels (Figure 11). Crossing of the lowest triplet radical pair energy level with the lowest radical pair energy level of the singlet results in an enhanced rate of intersystem crossing, producing a resonance
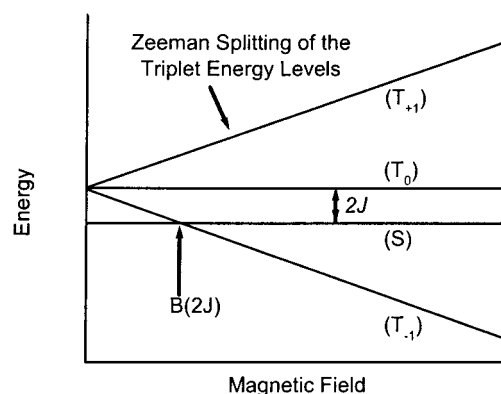

Figure 11. Radical ion pair energy levels as a function of magnetic field.

in the triplet yield at $B = 2J$. As the magnetic field is increased further, the energy gaps between the singlet and two of the three triplet radical pair energy levels increase. As a consequence, the overall triplet radical ion pair yield diminishes to a constant value determined by mixing of the singlet state (S) with the triplet state (T$_0$) that remains magnetic field invariant (Figure 11). Subsequent spin-selective radical ion pair recombination produces ^{3}(ZnTPP−PDI$_4$)$_n$, wherein the triplet excitation resides on PDI.

The observed resonance in the magnetic field effect on the ^{3}*PDI yield within the (ZnTPP−PDI$_4$)$_n$ nanoparticles (Figure 10) arises from production of a radical ion pair in which the average singlet−triplet splitting (spin−spin exchange interaction) $2J = 17$ mT. The value of $2J$ depends exponentially on the distance between the two radical ions, so that $2J$ is small when the distance r is large, and can be described by[55]

$$2J = 2J_0 \, e^{-\alpha(r-r_0)} \tag{1}$$

where $2J_0$ is the spin−spin exchange interaction at van der Waals contact, α is a constant, and r_0 is the van der Waals distance of about 3.5 Å. The spin−spin exchange interaction $2J$ is directly proportional to the electronic coupling matrix element V^2 for the charge recombination reaction.[56,57] In turn, electron transfer theory shows that the rate constant k_{ET} for electron transfer is directly proportional to V^2,[58,59] so that the exponential damping factor β for the distance dependence of the electron-transfer rate in eq 2 should be equal to α in eq 1.

It is well established that $\beta \cong 1.0$ Å^{-1} for electron transfer

$$k_{ET} = k_{ET}{}^0 \, e^{-\beta(r-r_0)} \tag{2}$$

through many organic molecules, so the same value can be used for α.[60,61] Using $2J = 17$ mT, $\alpha = 1.0$ Å^{-1}, $2J_0 = 9.5 \times 10^5$ T,[55] and $r_0 = 3.5$ Å, eq 1 predicts that $r = 21$ Å. However, the β values for electron transfer between molecules with interacting π systems may be somewhat lower. For example, we have

(50) Ford, W. E.; Kamat, P. V. *J. Phys. Chem.* **1987**, *91*, 6373−6380.
(51) Leenstra, W. R.; Gouterman, M.; Kwiram, A. L. *Chem. Phys. Lett.* **1979**, *65*, 278−280.
(52) Hasharoni, K.; Levanon, H.; Greenfield, S. R.; Gosztola, D. J.; Svec, W. A.; Wasielewski, M. R. *J. Am. Chem. Soc.* **1995**, *117*, 8055−8056.
(53) Hasharoni, K.; Levanon, H.; Greenfield, S. R.; Gosztola, D. J.; Svec, W. A.; Wasielewski, M. R. *J. Am. Chem. Soc.* **1996**, *118*, 10228−10235.
(54) Carbonera, D.; DiValentin, M.; Corvaja, C.; Agostini, G.; Giacometti, G.; Liddell, P. A.; Kuciauskas, D.; Moore, A. L.; Moore, T. A.; Gust, D. *J. Am. Chem. Soc.* **1998**, *120*, 4398−4405.

(55) De Kanter, F. J. J.; Kaptein, R.; Van Santen, R. A. *Chem. Phys. Lett.* **1977**, *45*, 575−579.
(56) Okamura, M. Y.; Isaacson, R. A.; Feher, G. *Biochim. Biophys. Acta* **1979**, *546*, 394.
(57) Nelsen, S. F.; Ismagilov, R. F.; Teki, Y. *J. Am. Chem. Soc.* **1998**, *120*, 2200−2201.
(58) Marcus, R. A. *J. Chem. Phys.* **1965**, *43*, 679−701.
(59) Jortner, J. *J. Chem. Phys.* **1976**, *64*, 4860−4867.
(60) Closs, G. L.; Miller, J. R. *Science (Washington, D.C.)* **1988**, *240*, 440−447.
(61) Moser, C. C.; Keske, J. M.; Warncke, K.; Farid, R. S.; Dutton, P. L. *Nature (London)* **1992**, *355*, 796−802.
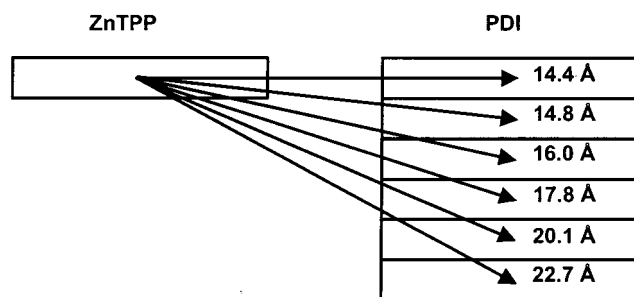
Figure 12. Schematic diagram showing the distances between a single ZnTPP and nearby PDI molecules within the (ZnTPP−PDI$_4$)$_n$ nanoparticles, assuming the structure given in Figure 5.

directly measured the distance dependence for electron transfer from guanine to photoexcited *trans*-stilbene within DNA hairpins for which $\beta = 0.6$.[62] Thus, $r = 21$ Å is most likely a lower limit for the average radical ion pair distance within the (ZnTPP−PDI$_4$)$_n$ nanoparticles. For example, if $\alpha = 0.6$ Å^{-1}, the same parameters predict that $r = 33$ Å. A minimum average radical ion pair distance of 21 Å implies that charge transport within the (ZnTPP$^+$−PDI$^-$$_4$)(ZnTPP−PDI$_4$)$_{n-1}$ nanoparticles occurs over distances that are substantially larger than the 14.4 Å ZnTPP−PDI distance within a single ZnTPP−PDI$_4$ molecule.

The question remains as to whether the holes or the electrons are more mobile within the nanoparticles. The transient absorption spectrum of (ZnTPP$^+$−PDI$^-$$_4$)(ZnTPP−PDI$_4$)$_{n-1}$ shown in Figure 8 suggests that PDI$^-$ interacts strongly with the other PDI molecules. Hole-hopping between guanines separated by 7 Å in DNA, the same distance as the assumed Zn−Zn interplanar spacing in (ZnTPP−PDI$_4$)$_n$, occurs at a relatively slow ($\sim 10^7$ s^{-1}) rate,[63] while high electron mobilities have been reported for stacked PDI molecules.[64] Taken together, these facts suggest that electron transport through the stacked PDI molecules most likely dominates in the (ZnTPP$^+$−PDI$^-$$_4$)(ZnTPP−PDI$_4$)$_{n-1}$ nanoparticles. Assuming the structure illustrated in Figure 5, the schematic diagram in Figure 12 shows the distances by which the charges are separated if the radical anion visits PDI sites in layers other than that in which it was generated. Using the ZnTPP radical cation as the origin, the average 21 Å distance (obtained from the magnetic field dependence of the triplet yield) places the electron on a PDI molecule that is five layers removed from the layer having the ZnTPP radical cation. The current data does not address the issue as to whether ^{3}*PDI, which is formed following charge recombination, also migrates through the structure.

The line width of the 2J resonance, $\Delta B \cong 2B_{1/2}$, typically depends on the magnitude of the hyperfine interactions within each radical of the pair, the distribution of 2J values that results from different radical ion pair distances, and uncertainty broadening due to the lifetime of the radical ion pair at a particular site. Anisotropic interactions, such as the dipolar interaction between the electron spins, as well as hyperfine anisotropy, are assumed to be negligible for the radical ion pairs studied here in solution.

(62) Lewis, F. D.; Wu, T.; Zhang, Y.; Letsinger, R. L.; Greenfield, S. R.; Wasielewski, M. R. *Science (Washington, D.C.)* **1997**, *277*, 673−676.
(63) Lewis, F. D.; Liu, X.; Liu, J.; Miller, S. E.; Hayes, R. T.; Wasielewski, M. R. *Nature* **2000**, *406*, 51−53.
(64) Struijk, C. W.; Sieval, A. B.; Dakhorst, J. E. J.; van Dijk, M.; Kimkes, P.; Koehorst, R. B. M.; Donker, H.; Schaafsma, T. J.; Picken, S. J.; van de Craats, A. M.; Warman, J. M.; Zuilhof, H.; Sudholter, E. J. R. *J. Am. Chem. Soc.* **2000**, *122*, 11057−11066.

An estimate of the contribution to $B_{1/2}$ due to the electron−nuclear hyperfine interactions of ZnTPP$^+$ ($a_N = 0.14$ mT, $a_H = 0.024$ mT) and PDI$^-$ ($a_N = 0.04$ mT, $a_H = 0.51, 0.59, 0.78$ mT) can be made using eqs 3 and 4:[65]

$$B_i = \left[\sum_k a_{ik}^2 I_k (I_k + 1) \right]^{1/2} \tag{3}$$

$$B_{1/2} = \frac{2(B_1^2 + B_2^2)}{B_1 + B_2} \tag{4}$$

where B_i is calculated for each radical i, a_{ik} are the hyperfine splittings, and I_k is the nuclear spin, and the summation runs over all nuclei with $I_k \neq 0$. This calculation gives $B_{1/2} = 1.1$ mT, which is about 60 times smaller than the experimental value of $B_{1/2} = 68$ mT. Thus, the contribution of the hyperfine interaction to the overall line width of the 2J resonance is very small.

Electron hopping between the stacked PDI molecules can contribute to the line width of the 2J resonance in two ways. First, hopping results in a distribution of radical ion pair distances, so that the steep exponential distance dependence of 2J produces large line width changes. Second, rapid hopping will lead to uncertainty broadening of the resonance due to the short residency time of the electron on each PDI. While the overall line width of the resonance is undoubtedly a convolution of these two sources of broadening, a simple analysis can evaluate in an approximate manner the relative contributions of both line-broadening mechanisms to the observed resonance line width. Equation 1 can be used to calculate 2J for radical ion pairs having the electron on sites immediately adjacent to the average site, i.e., $r = 21 \pm 3.5$ Å. Using $\alpha = 1.0$ Å^{-1}, 2$J_0 = 9.5 \times 10^5$ T, and $r_0 = 3.5$ Å, if $r = 17.5$ Å, then 2$J = 0.79$ T, whereas if $r = 24.5$ Å, then 2$J = 7 \times 10^{-4}$ T. These very large changes in 2J values suggest that the observed resonance line width most likely represents the population of radical ion pairs with the 21 Å average distance, while the remaining population contributes to the broad wings of the resonance. Thus, if the observed resonance line width $\Delta B \cong 2B_{1/2}$ for the population of radical ion pairs with the 21 Å average distance is attributed entirely to uncertainty broadening,[66] where $\Delta B \tau \cong \hbar$ and $\hbar = 5.7 \times 10^{-12}$ T·s, then the predicted site-to-site hopping rate $1/\tau = 2.4 \times 10^{10}$ s^{-1}. This rate is about 200 times faster than the overall 7.2 ns charge recombination rate of the (ZnTPP$^+$−PDI$_4^-$)(ZnTPP−PDI$_4$)$_{n-1}$ radical ion pairs. This result is consistent with a kinetic simulation of the equilibria for site-to-site hopping between the six PDI molecules in the array shown in Figure 12 (see Supporting Information).

Conclusions

The self-assembly of ZnTPP−PDI$_4$ into (ZnTPP−PDI$_4$)$_n$ nanoparticles is driven primarily by a strong van der Waals interaction between the PDI molecules. The PDI chromophores provide dual antenna and charge carrier functions that are analogous to the roles of chlorophyll within photosynthetic proteins. Photoexcitation of these nanoparticles initiates an ultrafast charge separation that occurs with near unit efficiency yet results in migration of the electron between several closely

(65) Weller, A.; Nolting, F.; Staerk, H. *Chem. Phys. Lett.* **1983**, *96*, 24−27.
(66) Staerk, H.; Treichel, R.; Weller, A. *Chem. Phys. Lett.* **1983**, *96*, 28−30.

coupled electron acceptors, a process that is more closely analogous to dye-sensitized charge injection into semiconductors than to stepwise photosynthetic electron transport. The hybrid nature of charge generation and transport within these nanoparticles should prove useful for developing insights into solid-state device structures for photoconversion.

Experimental Section

Solid Film Preparation and Characterization. Quartz plates (Chemglass) were cleaned by immersion in a freshly prepared piranha solution (concentrated H_2SO_4:30% H_2O_2 = 7:3 v/v) at 80 °C for at least 45 min. ***Caution!*** *This solution is an extremely strong oxidizing agent.* After cooling to room temperature, the slides were rinsed repeatedly with deionized (DI) water, subjected to an RCA-type cleaning procedure (H_2O:30% H_2O_2:NH_4OH = 5:1:1 v/v/v), and sonicated at room temperature for 45 min. The substrates were then rinsed with DI water and dried in an oven overnight at 115 °C. The freshly cleaned substrates were placed in an oven-dried Schlenk-type reactor. A 50 mM solution of CH_3SiCl_3 in dry toluene solution was added and reacted for 5 h at 25 °C. The solution was then removed with a canulla. The functionalized substrates were washed twice with toluene, acetone, and methanol and dried under vacuum. A 10^{-4} M toluene solution of $(ZnTPP-PDI_4)_n$ was spin-coated (Laurell WS-400) onto the quartz substrate at 2000 rpm for 30 s, dried at room temperature under N_2, and stored in the dark under N_2 until use. The $(ZnTPP-PDI_4)_n$ film on the quartz substrate was examined by tapping-mode atomic force microscopy using a Digital Instruments Multimode Nanoscope IIIa. Optical absorption spectra of the film were recorded on the instrument described below.

Spectroscopy. Femtosecond transient absorption measurements were made using a regeneratively amplified titanium:sapphire laser system operating at a 2 kHz repetition rate.[48] The frequency-doubled output from the laser was used to provide 420 nm, 130 fs pulses for excitation, while 515 nm, 130 fs excitation pulses were produced using an optical parametric amplifier.[67] A white light continuum probe pulse was generated by focusing the 840 nm fundamental into a 1 mm sapphire disk. Cuvettes with a 2 mm path length were used, and the samples were bubbled with N_2 and irradiated with 0.5 μJ per pulse focused to a 200 μm spot. The optical density at the excitation wavelength was typically 0.3–0.5. The samples were stirred during the experiment using a wire stirrer to prevent thermal lensing and sample degradation. The total instrument response for the pump–probe experiments was 180 fs.

Nanosecond transient absorption measurements were made using the 416 nm, H_2-Raman shifted output from a frequency-tripled 10-Hz Nd: YAG laser (QuantaRay DCR-2). Probe light was generated using a xenon flashlamp (EG&G Electro-optics FX-200, 60 μs) and detected using a photomultiplier tube with voltage applied to only four dynodes (Hamamatsu R928). The total instrument response was 7 ns and is determined primarily by the laser pulse duration. The samples were placed in a 10 mm quartz cuvette equipped with a vacuum adapter and subjected to five freeze−pump−thaw degassing cycles prior to the transient absorption measurements. The cuvette was placed between the poles of a Walker Scientific HV-4W electromagnet powered by a Walker Magnion HS-735 power supply. The field strength was measured by a Lakeshore 450 gaussmeter with a Hall effect probe. Both the electromagnet and the gaussmeter were interfaced with the data collection computer, allowing measurement and control of the magnetic field to $\pm 1 \times 10^{-5}$ T during data acquisition. The optical density of all samples was maintained between 0.7 and 1.0 at 416 nm. Thirty shots were averaged at each magnetic field strength with a LeCroy 9384 digital oscilloscope and sent to the computer, which calculated the ΔA. The relative triplet yield reported is $T/T_0 = \Delta A(B)/\Delta A(B = 0)$. The results presented are an average of three experiments conducted on separate days with freshly prepared samples. Kinetic analyses were performed at several wavelengths using a nonlinear least-squares fit either to a general sum-of-exponentials function or to a series $A \rightarrow B \rightarrow C$ kinetic mechanism using the Levenberg−Marquardt algorithm.

Steady-state absorption spectra were obtained in 1 cm path length cuvettes using a Shimadzu 1601 UV−vis spectrophotometer. Nanoparticle size measurements in solution were performed using a Coulter N4-Plus dynamic laser light-scattering apparatus with a 632.8 nm He−Ne laser source.

Electrochemistry. Electrochemical measurements were performed using a CH Instruments model 660A electrochemical workstation. The solvents were butyronitrile (PrCN) and methylene chloride containing 0.1 M tetra-n-butylammonium perchlorate electrolyte. A 1.0 mm diameter platinum disk electrode, platinum wire counter electrode, and Ag/Ag$_x$O reference electrode were employed. Ferrocene/ferrocinium (Fc/Fc$^+$, 0.52 vs SCE) was used as an internal reference for all measurements. Spectroelectrochemical measurements were performed in a 1 mm path length quartz cell with a threaded top. A Teflon reservoir was outfitted to thread onto the quartz cell. The platinum counter electrode and silver wire reference electrode were placed in the reservoir, which held a solution of 0.1 M tetra-n-butylammonium perchlorate in DMF. The working electrode was an optically transparent platinum wire mesh inserted into the 1 mm cuvette. The electrochemical workstation controlled the potential of the working electrode, and a Shimadzu 1610A UV−vis spectrometer obtained the absorption spectra of the redox species. All electrochemical measurements were carried out under a blanket of argon.

Supporting Information Available: Details regarding the synthesis and characterization of the molecules used in this study as well as kinetic simulations (PDF). This material is available free of charge via the Internet at http://pubs.acs.org.

(67) Greenfield, S. R.; Wasielewski, M. R. *Opt. Lett.* **1995**, *20*, 1394−1396.

JA026286K